

# Orbits of Four Very Massive Binaries in the R136 Cluster

Philip Massey<sup>1</sup>

*Lowell Observatory, 1400 West Mars Hill Road, Flagstaff, AZ 86001*

`massey@lowell.edu`

Laura R. Penny

*Department of Physics and Astronomy, College of Charleston, 66 George Street,  
Charleston, SC 29424*

`pennyl@cofc.edu`

and

Julia Vukovich<sup>2</sup>

*Lowell Observatory, 1400 West Mars Hill Road, Flagstaff, AZ 86001*

## ABSTRACT

We present radial velocity and photometry for four early-type, massive double-lined spectroscopic binaries in the R136 cluster. Three of these systems are eclipsing, allowing orbital inclinations to be determined. One of these systems, R136-38 (O3 V + O6 V), has one of the highest masses ever measured,  $57M_{\odot}$ , for the primary. Comparison of our masses with those derived from standard evolutionary tracks shows excellent agreement. We also identify five other light variables in the R136 cluster which are worthy of follow-up study.

*Subject headings:* stars: early-type—binaries: spectroscopic—binaries: eclipsing—stars: evolution—Magellanic Clouds

---

<sup>1</sup>Based on observations made with the NASA/ESA Hubble Space Telescope, obtained at the Space Telescope Science Institute, which is operated by the Association of Universities for Research in Astronomy, Inc., under NASA contract NAS 5-26555. These observations are associated with proposal 8217.

<sup>2</sup>Participant in the National Science Foundation's Research Experience for Undergraduates (REU) program, summer 2001. Current affiliation: Wichita State University

## 1. Introduction

Empirical checks on the mass-luminosity relation and on how well the evolutionary models match reality are sorely lacking for high mass ( $> 20\mathcal{M}_{\odot}$ ) stars, even near the zero-age main-sequence (ZAMS). It has long been recognized that evolutionary tracks (past the ZAMS) are affected by mass-loss (see, for example, Brunish & Truran 1982), and it is now well recognized that in particular the models are highly sensitive to how mixing of material to and from the core is treated (Maeder & Conti 1994), with the most recent work emphasizing the importance of rotation in this regard (Meynet & Maeder 2000; Maeder & Meynet 2000; Heger & Langer 2000; Heger, Langer, & Woosley 2000). Yet these models, untested as they may be, provide the only means for linking a variety of observational studies to astrophysical interpretation, such as the determination of the initial mass function (Massey 1998) and the determination of turn-off masses in clusters containing massive stars (Massey, Waterhouse, & DeGioia-Eastwood 2000, Massey, DeGioia-Eastwood, & Waterhouse 2001).

Herrero et al. (1992) first called attention to a significant *mass discrepancy* between the masses derived from modern stellar atmosphere models, and that inferred from stellar evolution codes, for the highest mass stars, in the sense that the evolutionary tracks predict a mass as much as 2 times larger. (See also Herrero, Puls, & Villamariz 2000.) Burkholder, Massey, & Morrell (1997) recently tried to resolve this mass discrepancy by using data on massive spectroscopic binaries. They found good agreement between the binary masses and the evolutionary tracks up to  $25\mathcal{M}_{\odot}$ . Some higher mass systems did show significant lower masses than the evolutionary tracks would suggest, but these systems were either at or near their Roche lobes, suggesting that significant mass might have been lost from the system. (See also Penny, Gies, & Bagnuolo 1999.)

Massey & Hunter (1998) recently obtained spectra of 65 of the bluest, most luminous stars in the R136 cluster located at the heart of the 30 Doradus nebula in the LMC. The majority of these stars proved to be of spectral type O3, the hottest, most luminous, and most massive stars known. Four of the stars showed widely spaced, double absorption lines, indicative of spectroscopic binaries caught at favorable phases. Since the evolutionary masses of these stars were very high, it was thought that these would be excellent candidates for additional study, in the hopes that orbit solutions would resolve the mass discrepancy once and for all.

## 2. Observations and Reductions

### 2.1. The Data

The data were all obtained as part of a Cycle 8 *HST* program, GO-8217. We utilized 30 orbits, organized into 15 “visits” of 2 consecutive orbits, with each visit separated by carefully planned intervals. We used the Space Telescope Imaging Spectrograph (STIS) in imaging mode for photometry of our binaries, and with a medium-dispersion grating for spectroscopy of each binary.

Each visit began with a pair of short images (total integration time of 2.2 seconds) obtained with the “long-pass” filter (which cuts off all light  $< 5500\text{\AA}$ ) and centered on the middle of the cluster. The 28 arcsec by 51 arcsec field of view always contained our four binaries, but changes in the spacecraft roll angle resulted in some of the out-lying R136 stars either being included or not. The spatial scale was 0.05 arcsecs per pixel.

After centering up on a fairly isolated offset star (Melnick 34 = R136-8; see Fig. 1 of Massey & Hunter 1998), the telescope was precisely offset to each of the four binaries in turn, in order to obtain spectra with the G430M grating centered at  $\lambda 4451$ . These exposures covered the wavelength range  $4310\text{\AA}$  to  $4590\text{\AA}$  at a dispersion of  $0.28\text{\AA}$  per pixel, with a nominal 1.5-pixel resolution of  $0.42\text{\AA}$  ( $28 \text{ km s}^{-1}$ ). This wavelength region was selected to include as many spectral lines as possible in a single wavelength setting; i.e.,  $\text{H}\gamma$ , He I  $\lambda 4471$ , and He II  $\lambda 4542$ . We used the 0.2 arcsec by 52 arcsec slit. Wavelength calibration was obtained for each exposure using the default *HST*/STIS scheme, resulting in a new calibration exposure prior to the first spectroscopic exposure for each orbit.

Near the end of each visit, another pair of short-exposure images (total integration time 2.6 seconds) were obtained to continue the photometric monitoring. The total elapsed time for each visit was 3.2 hours.

In order to maximize our phase coverage for all periods of interest, we adopted a clever scheme developed by Abi Saha for observing Cepheids as part of the distance-scale key project: we designed our program so that each visit was separated in time according to a geometrical progression, corresponding to

$$\text{gap}(n)[\text{days}] = 0.5 * 1.175^n, n = 1, 14$$

The multiplicative and geometrical factors are chosen to assure good phase coverage for the shortest and longest periods of interest, given a predetermined number of observations. Simulations showed that this would provide uniformly good phase coverage for periods from

$< 1$  day through 30 days. The longest interval between successive visits was 3.7 days, and the shortest interval was 0.5 days. The observations spanned an observing “season” of 24.4 days. In arranging the order of our visits, we put all the shorter intervals near the middle of the 24 day sequence, with progressively longer intervals to either end. The result of this is that any eclipses would tend to be found in the middle of the sequence, as we will find in Sec. 3.6 is indeed the case.

## 2.2. Photometry

For the STIS images, we used the “standard pipeline” flat-fielded images prior to cosmic-ray (CR) rejection. They had been observed in “CR-split” mode, resulting in a pair of images, each of 1.1–1.3 sec duration. We chose to do photometry of all 60 images, and rejected CR events by comparing the photometry from each of the CR-split images. If the photometry agreed to within the photometric errors ( $3\sigma$ ), we averaged the results; if not, we assumed that the smaller magnitude was spurious due to a CR event. The photometry was measured using IRAF’s aperture photometry routine, with a radius of 2 pixels and sky being determined from the modal value within an annulus lying 5–10 pixels from the star’s center. The point-spread-function has a full-width at half-radius of 1.7 pixels, and we found that the centers were well determined by a Gaussian fit to the radial profile.

In order to provide more accurate differential photometry for our binaries, and to search for other light variables, we performed photometry of 59 of the brightest, most isolated stars in the cluster, including our four binaries. Of the 59 stars, one happened to lie outside the field-of-view for two of the visits, due to the slightly changing roll-angle of the spacecraft over the course of the observations. After eliminating possible variables (based upon whether agreement frame-to-frame was within the photometric errors), we found that there were indeed photometric zeropoint changes of  $\sim 0.04$  mag from frame-to-frame, with the drifts being secular rather than random in time: i.e., over the course of several days the zero-point would drift upwards and then downwards again. This is consistent with the claim that “instrumental [in]stability” limits absolute photometry with STIS to 5% (Table 16.3 in Leitherer et al. 2001). In any event, our use of STIS as an N-star photometer (with  $N \sim 58 - 59$ ) resulted in photometry with high precision for temporal changes.

We have applied a single adjustment to the photometric zero-point to have the photometry roughly match  $V$ ; a single value worked well as the colors of these stars are all very similar (Hunter et al. 1997).

### 2.3. Spectroscopy

Owing to the extreme crowding in the R136 cluster, the spectra for each of the four binaries had to be re-extracted with a small aperture centered on each target, with care being taken to select “clean” sky on either side of the slit. We actually reduced our spectra two ways. For one version, we began with the pipeline final two-dimensional spectrum (flat-fielded, CR-removed, geometrically-corrected, and wavelength calibrated) and simply re-extracted the spectra of our binaries. For the other, we began with the flat-fielded version, and extracted our spectra using the usual IRAF routines; for these we also applied our own dispersion solution determined from the wavelength-calibration frames. We found in practice that our own reductions provided better signal-to-noise.

In measuring the spectra, we fit double lines using two Vogt functions; this provided excellent fits to even blended double lines, and avoids issues with pair-blendings, always a concern with orbit solutions of broad-lined stars (see discussion in Burkholder et al. 1997). The single-lined phases were measured with a single Vogt function for consistency. Both versions of the spectra were measured independently, and the results compared; no systematic differences were found, and the comparison proved useful mainly for eliminating any spurious measurements due to noise spikes. Our measuring error was 5-10 km s<sup>-1</sup>.

## 3. Results

We provide the photometric data and radial velocity data in Tables 1 and 2. In this section we describe what we learned from the spectra of each binary, and provide details of the orbit solutions and analysis of the light-curve information. We also report the discovery of five more light-variables in the R136 cluster. We begin by explaining our methods.

### 3.1. Methodology

For the period searches, we used a version of the Lafler & Kinman (1965) routine, which relies upon point-to-point smoothness after the data (either photometric or radial velocity) are sorted in phase according to a trial period. For the orbit solutions, we initially solved for each component independently using a modified version of the differential corrections program of Wolfe, Horak, & Storer (1967), fixing only the period. In all cases we found solutions consistent with circular orbits, which we expect given the short periods and high masses (see Sect. 4). We then determined the best values of the orbital semi-amplitudes  $K$  “center-of-mass”  $\gamma$ -velocities by running a non-linear least-square routine based upon the

grid-search program of Bevington’s (1969), with the eccentricity, time of conjunction, and periods fixed for the two components. This then maximizes the precision of our determination of  $\gamma$  and  $K$ . As a reminder, we expect that the  $\gamma$ -velocities of the two components of a massive binary will differ due to the photospheric outflow velocities of the stellar winds (Massey & Conti 1977). We characterize the agreement between the orbit and velocity data by R1, computed from the goodness-of-fit  $\chi$ .

The spectral types and magnitude difference between the components can be determined from the best double-lined phases. Our spectral types differ slightly from those of Massey & Hunter (1998), as these STIS spectra have considerably higher resolution and better signal-to-noise. The relative strengths of He II  $\lambda 4542$  and He I  $\lambda 4471$  helped establish the spectral class; the absolute visual magnitudes were consistent with all of these stars being dwarfs. The magnitude difference could be measured from the relative fluxes of the H $\gamma$  lines at double-lined phases, as the equivalent width of H $\gamma$  is fairly insensitive to  $T_{\text{eff}}$  for dwarfs this hot.

We measured the projected rotation velocity  $v \sin i$  for each component by using the appropriate model atmosphere lines and convolving these with rotational velocities until we obtained the best fit to a line. The model atmosphere code is that described by Kudritzki & Puls (2000), and we used models computed by PM for stars of similar spectral types in the LMC. Given the intrinsic line widths, we found we could not measure rotational velocities smaller than 90-100 km s $^{-1}$ . In the following, we will compare the rotational velocities to that expected on the basis of synchronous rotation, computed using the stellar radii and orbital period.

We thus know a great deal about the physical parameters of these stars, which is helpful in reducing the number of free parameters in interpreting the light-curves. We adopt a distance modulus  $(m - M)_o = 18.5$ , in accord with Westerlund (1997) and van den Bergh (2000). Accurate values of the reddening were determined by Massey & Hunter (1998) based upon the multi-band *HST* photometry of Hunter et al. (1997). Thus the absolute visual magnitudes are known (Table 1 of Massey & Hunter 1998) for the combined systems, and, combined with the magnitude differences measured from the spectra, tells us  $M_V$  for each component in the binary. The spectral type allows us to assign effective temperatures; we adopt the scale of Chlebowski & Garmany (1991). (We will discuss this in more detail in Sec. 4.) The effective temperature then determines the bolometric correction (Vacca, Garmany, & Shull 1996), and hence we know the bolometric luminosity of each star.

We used the light curve synthesis code GENSYN (Mochnicki & Doughty 1972) to produce model light curves. Our approach was to make a constrained fit using as much data as possible from the spectroscopic results as described above. The orbital parameters were

taken from the spectroscopic solution, and the physical parameters were estimated from the spectral classifications of the stars. We set the stellar temperatures according to the spectral classification. We then estimated the physical fluxes and limb darkening coefficients from tables in Kurucz (1979) flux models and Claret (2000), respectively. The observed flux ratios together with the adopted effective temperatures yield estimates of the ratio of stellar radii. Then, for a given input value of the polar radius of the primary  $R_p$ , we calculated the secondary radius. Each trial run of GENSYN was set by two independent parameters, the system inclination  $i$  and primary polar radius. For each run, we attempt to match two observables: the absolute visual magnitude of the system and the eclipse depths and widths. The best fit solutions are those with the calculated  $M_V$  of the system that also matched the eclipse depths. Models that fit the eclipse depths could be made for a range of inclinations, however the  $M_V$  for such models would greatly diverge from that calculated using the well known distance and reddening to the LMC. The quoted errors in inclination derive from an estimated error of  $\pm 0.15$  mag on our  $M_V$  values, which is based upon the uncertainty in the LMC distance modulus (van den Bergh 2000) and a modest error in the photometry and reddening (Massey & Hunter 1998).

For all four systems, the stars are well contained within their Roche surfaces. In the case of R136-39, no eclipses are seen. However, the crucial phases where we might expect eclipses lack observations. Therefore, we only quote an upper limit on the inclination. Any inclination above this value would result in eclipses that would be both too deep and wide to agree with the current observations.

As a further check on the models, we independently estimated the orbital inclination simply from geometry, after measuring the eclipse depths. For this, we adopt a modest correction for limb darkening using a linear coefficient (Al-Naimiy 1978; van Hamme 1993), but ignore reflection and other second-order effects. Given the poor sampling in phase-space we expected only modest agreement with the models, but in fact the agreement was excellent, giving us high confidence that the orbital inclinations are well determined.

We estimate the errors on the physical parameters, including a 10% uncertainty in the effective temperature scale for O-type stars (Conti 1988). Nevertheless, our parameters are well determined, in large part because the inverse dependence of the stellar radii on effective temperature is partially canceled by the dependence of the bolometric correction on effective temperature, and in fact the uncertainties in  $\Delta m$  dominate the errors on the stellar radii.

$$\begin{aligned} L/L_\odot &= (R/R_\odot)^2 \times (T_{\text{eff}}/T_\odot)^4 \\ R/R_\odot &= (L/L_\odot)^{0.5} \times (T_\odot/T_{\text{eff}})^2 \end{aligned} \tag{1}$$

For solar-type stars, a small error in estimating the effective temperature  $T_{\text{eff}}$  would result in a large error in  $R/R_\odot$ , since there is such a steep inverse relationship with  $T_{\text{eff}}$ . However,

for hot stars we must make a very large correction for the bolometric correction (BC) in determining  $L/L_\odot$  starting with  $M_V$ , and that the BC has a very steep dependence on  $T_{\text{eff}}$  as well:

$$\text{BC} = 27.66 - 6.84 \times \log T_{\text{eff}},$$

from Vacca et al. (1996). Thus substituting this into equation (1), and adopting  $T_\odot = 5770^\circ\text{K}$ , we find

$$R/R_\odot = 871.67 \times 10^{-M_V/5} \times T_{\text{eff}}^{-0.632}.$$

By propagation of errors we find then that

$$\sigma_{R/R_\odot}^2 = \sigma_{T_{\text{eff}}}^2 \times (-550.90 \times 10^{-M_V/5} \times T_{\text{eff}}^{-1.632})^2 + \sigma_{M_V}^2 \times (-401.42 \times 10^{-M_V/5} \times T_{\text{eff}}^{-0.632})^2$$

### 3.2. R136-38

Six of the 15 spectra showed double lines at  $\text{H}\gamma$  and  $\text{He II } \lambda 4542$ . There is a large magnitude difference between the two components, which we measure as  $\Delta m = 1.0 \pm 0.2$  mag. The  $\text{He I } \lambda 4471$  line clearly follows the motion of the secondary, but never showed any component due to the primary. Thus we have a good measurement of the motion of the secondary for both single-lined and double-lined phases. Occasionally the  $\text{He I}$  line was too noisy to measure. We find that the single-lined phases follow the motion of the primary very well, but we will not give those any weight in the orbit solutions. The primary is of spectral type O3 V, while the secondary is of spectral type O6 V, as judged by the relative strengths of  $\text{He I}$  and  $\text{He II}$  during the double-lined phases. The photometry shows well pronounced dips of  $\sim 0.2$  mag indicative of eclipses.

Period searches on the radial velocity data (both primary and secondary) and on the photometry all revealed the same period, 3.39 days. We present the orbital parameters in Table 3, and show the radial velocity curves and orbit fit in Fig 1. We find that the rotational velocities are consistent with synchronous rotation. Analysis of the light-curve finds a well-determined orbital inclination of  $i = 79^\circ \pm 1^\circ$ . We show the light curve data, and the model fit, in Fig 1 as well.

This is a very interesting system, containing stars of extremely high masses, with the O3 V primary having a mass of  $57M_\odot$ . This is higher than the mass determined from any other binary, exceeding the mass of even that of Plaskett’s star ( $51M_\odot$ , Bagnuolo, Gies, & Wiggs 1992).<sup>3</sup> We compare these to the masses derived from the evolutionary tracks in Table 3, and find excellent agreement.

---

<sup>3</sup>There are two other contenders for the recorder-holder. (1) HD 92740 is a WN7 Wolf-Rayet star in

### 3.3. R136-39

This system consists of an O3 V + O5.5 V pair. Of the 15 spectra, 11 show double lines at  $H\gamma$  and He II  $\lambda 4542$ , and it is clear the He I  $\lambda 4471$  comes purely from the secondary. The magnitude difference between the two components is  $0.45 \pm 0.1$  mag. The period is 4.06 days, as determined from the radial-velocities. Inspection of the unphased photometry did not show any obvious signs of an eclipse, but when phased according to the radial velocity information we find that there is poor coverage near the important phases. This allows us only to assign an upper limit on  $i$ , and our modeling suggests that the orbital inclination must be less than  $75^\circ$  to account for the lack of deeper eclipses. This places only lower limits on the masses on the system, of  $27M_\odot$  and  $21M_\odot$ . The line widths are consistent with synchronous rotation.

### 3.4. R136-42

This system consists of an O3 V + O3 V pair. Of the 15 spectra, 11 showed double lines at  $H\gamma$  and He II  $\lambda 4542$ , and there was no trace of He I in any of our spectra. The magnitude difference between the two components is modest,  $\Delta m = 0.2 \pm 0.1$ . The light-curve shows a very deep eclipse (0.5 mag), suggesting that we are viewing this system at a very favorable inclination.

A period search of both the radial velocity and photometry data yielded the same value,  $P = 2.89$  days. We give the orbital parameters in Table 5, and show the orbit and light-curve in Fig. 3. We find  $i = 85.4^\circ$ . The masses are among the highest seen in a spectroscopic binary,  $40M_\odot$  and  $33M_\odot$ . The line widths are consistent with synchronous rotation.

### 3.5. R136-77

The last system we discuss consists of two O5.5 V + O5.5 V stars with equal brightness. Of the 15 spectra, 12 showed double lines at  $H\gamma$ , He I  $\lambda 4471$ , and He II  $\lambda 4542$ . However,

---

which the absorption lines and emission lines follow the same orbital motion. By combining spectra from six He I lines, Schweickhardt et al. (1999) report the detection of a secondary absorption spectrum, which they describe as O9 III. The double-lined orbit solution yields a mass of  $55.3 \pm 7.3M_\odot$  for the Wolf-Rayet star. (2) HD 93205 is an O3 V + O8 V pair recently studied by Antokhina et al. (2000). The mass of the O3 V primary was found to be  $32\text{--}154M_\odot$ , with a most probable value of  $45M_\odot$ . We are indebted to Doug Gies for reminding us of these systems.

since we could not distinguish the primary from the secondary, it was necessary to rely upon the velocity *differences* between the two components in order to find the period; a period search of the photometry yielded identical results, and strong (0.4 mag) eclipses are evident. The period was then used to phase the radial velocity data, and assign velocities to one star or the other. We designate the slightly more massive star the primary. The radial velocity data, orbit solution, and light-curve is shown in Fig. 4. The line widths are again found to be consistent with synchronous rotation.

### 3.6. Other Light Variables

In doing the photometry, we found five additional stars with significant photometric variations. We show the light-curves in Fig. 5. R136-07 (Melnick 39), R136-15 (Melnick 30), R136-24 (R136a7), and R136-25 all show signatures of what might well be eclipses. The star R136-08 (Melnick 34) shows a much more puzzling behavior, changing by several tenths of a magnitude over the course of 3 weeks. The variations appear to be periodic. The spectrum of R136-08 mimics that of a Wolf-Rayet star, although Massey & Hunter (1998) argue that it is simply a “super Of” star whose very high luminosity and stellar winds result in a spectrum dominated by emission. Spectroscopic and photometric monitoring of all five of these stars has been proposed for Cycle 11 with *HST*.

## 4. Discussion

Our analysis of the four R136 binaries have revealed orbital masses that are among the highest ever directly measured via this simple application of Kepler’s second law. We can use these new data to compare to the masses derived from the evolutionary tracks<sup>4</sup>. We have included these values in Tables 3-6, and present the H-R diagrams (HRDs) in Fig 6. The agreement between the masses derived from these tracks, and the actual measured masses, is excellent for the three cases with eclipses.

In placing the stars in the H-R diagram, we have chosen to adopt the effective temperature scale of Chlebowski & Garmany (1991). This is similar to the scale given by Conti (1988), who provides a critical discussion, and concludes that the absolute (but not relative)

---

<sup>4</sup>We have used the older Schaerer et al. (1993) evolutionary tracks as these were the last set made public by the Geneva group that includes normal (rather than enhanced) mass-loss rates. Newer models including rotation are becoming available, but as yet none with the metallicity appropriate to the LMC. However, we expect that this effect will be small *near the ZAMS*, as suggested by Fig. 6 in Maeder & Meynet (2001).

uncertainties in the scale are about 10%. Since that time, more modern atmospheric models have been used to analyze a number of O-type stars in the Milky Way, LMC, and SMC; see, for example, Puls et al. (1996). Such studies led Vacca et al. (1996) to propose a new effective temperature scale, which is  $\sim 6\%$  hotter than the Conti (1988) calibration, and  $\sim 3\%$  hotter than the Chlebowski & Garmany (1991) scale for the spectral types discussed in the current paper. We note that there are no spectral type to effective temperature scales determined for stars in the LMC and SMC, and that Vacca et al. (1996) restricted their study to Galactic stars. Thus refinements in the effective temperature scale will change the location of the stars in the HRD but probably the error bars in Fig. 6 are realistic. Note that we have only included the uncertainty in  $M_V$  in estimating the errors on the evolutionary track masses in Tables 3-6; were we to include the uncertainty in the effective temperature scale as well, the percentage error would roughly double.

The stars do fall slightly to the left of where we expect in the HRDs. Massey & Hunter (1998) found ages of 1-2 Myr for the R136 cluster, with the larger value corresponding to the cooler effective temperature scale, which we have used here. Yet the components in all four of our binaries lie on or near the ZAMS, to higher effective temperatures than the 2 Myr isochrones shown in Fig. 6. We do not have a ready explanation for this. We note that all four of these systems are relatively close pairs. Comparison of the orbital separations  $a \sin i$  with the stellar radii (both quantities appear in Tables 3-6) reveals that the components are typically separated by  $\sim 2 \times$  the sum of the radii. This is sufficiently close that tidal forces have played a significant role. We see ready evidence of this in that there must have been some dynamical evolution for the orbits to be circular and the stars to be locked in synchronous rotation.<sup>5</sup> Such tidal forces may have affected the evolution of the stars (providing additional heating on the envelopes), and in that case, these systems are not telling us as much as we would like about single stars. It is hoped that some of the stars identified in Sect. 3.6 may provide example of massive binaries with longer periods.

Such systems would also help determine if the new generation of rotating stellar models do better than the standard non-rotating models. Maeder & Meynet (2000) have recently invoked rotation to explain the discrepancy in masses between the evolutionary tracks and stellar atmosphere calculations; they note that tracks which fail to include rotation may overestimate the mass by as much as 50% in cases of high rotation and luminosity. The short periods of our binaries have resulted in slow rotation due to tidal forces, leading to little difference in the masses predicted by non-rotating and rotating models.

---

<sup>5</sup>The time expected for tidal forces to circularize an orbit can be estimated using equation (2) of Shu & Lubow (1981); adopting parameters appropriate to high-mass stars with convective cores (Zahn 1975, 1977) leads to  $\sim 500,000$  years for these systems.

We are grateful to Abi Saha for extensive discussions of how best to observe variable objects in order to obtain good phase coverage. In order to measure the rotational velocities of the stars, we used the model atmosphere code of Rolf Kudritzki and his collaborators. We thank Deidre Hunter for a critical reading of the manuscript, and Andy Odell for an interesting conversation about one of these stars. Kim Venn provided useful suggestions for improving the paper. Support for REU student JV was provided by NSF grant 9988007. *HST* proposal GO-8217 was provided by NASA through a grant from the Space Telescope Science Institute, which is operated by the Association of Universities for Research in Astronomy, Inc., under NASA contract NAS 5-26555.

## REFERENCES

- Al-Naimiy, H. M. 1978, *Ap&SS*, 53, 181
- Antokhina, E. A., Moffat, A. F. J., Antokhin, I. I., Bertrand, J.-F., & Lamontagne, R. 2000, *ApJ*, 529, 463
- Bagnuolo, W. G., Gies, D. R., & Wiggs, M. S. 1992, *ApJ*, 385, 708.
- Bevington, P. R. 1969, *Data Reduction and Error Analysis for the Physical Sciences* (New York: McGraw-Hill)
- Brunish, W. M., & Truran, J. W. 1982, *ApJ*, 256, 247
- Burkholder, V., Massey, P., & Morrell, N. 1997, *ApJ*, 490, 328
- Chlebowski, T., & Garmany, C. D. 1991, *ApJ*, 368, 241
- Claret, A. 2000, *A&A*, 363, 1081
- Conti, P. S. 1988, in *O Stars and Wolf-Rayet Stars.*, ed. P. S. Conti & A. B. Underhill, NASA SP-497 (Washington, DC: NASA), 124
- Heger, A., & Langer, N. 2000, *ApJ*, 544, 1016
- Heger, A., Langer, N., & Woosley, S. E. 2000, *ApJ*, 528, 368
- Herrero, A., Kudritzki, R. P., Vilchez, J. M., Kunze, D., Butler, K., & Haser, S. 1992, *A&A*, 261, 209
- Herrero, A., Puls, J., & Villamariz, M. R. 2000, *A&A*, 354, 193
- Hunter, D. A., Vacca, W. D., Massey, P., Lynds, R., & O’Neil, E. J. 1997, *AJ*, 113, 1691
- Kudritzki, R.-P., & Puls, J. 2000, *ARA&A*, 38, 613
- Kurucz, R. L. 1979, *ApJS*, 40, 1
- Laffer, J., & Kinman, T. D. 1965, *ApJS*, 11, 216
- Leitherer et al. 2001, *STIS Instrument Handbook*, Version 5.1 (Baltimore: STScI)
- Massey, P. 1998, in *The Stellar Initial Mass Function*, 38th Herstmonceux Conference, ed. G. Gilmore & D. Howell, (San Francisco, ASP), 17
- Massey, P., & Conti, P. S. 1977, *ApJ*, 218, 431
- Massey, P., & Hunter, D. A. 1998, *ApJ*, 493, 180
- Massey, P., DeGioia-Eastwood, K., and Waterhouse, E. 2001, *AJ*, 121, 1050
- Massey, P., Waterhouse, E., and DeGioia-Eastwood, K. 2000, *AJ*, 119, 2214
- Maeder, A., & Conti, P. S. 1994, *ARA&A*, 32, 227

- Maeder, A., & Meynet, G. 2000, *ARA&A*, 38, 143
- Maeder, A., & Meynet, G. 2001, *A&A*, 373, 555
- Meynet, G., & Maeder, A. 2000, *A&A*, 361, 101
- Mochnicki, S. W., & Doughty, N. A. 1972, *MNRAS*, 156, 51
- Penny, L. R., Gies, D. R., & Bagnuolo, W. G. 1999, in *Wolf-Rayet Phenomena in Massive Stars and Starburst Galaxies*, ed. K. A. van der Hucht, G. Hoenigsberger, & P. R. J. Eenens (San Francisco, ASP), 86
- Puls, J., Kudritzki, R. P., Herrero, A., Pauldrach, A. W. A., Haser, S. M., Lennon, D. J., Gabler, R., Voels, S. A., Vilchez, J. M., Wachter, S., & Feldmeier, A. 1996, *A&A*, 305, 171
- Schaerer, D., Meynet, G., Maeder, A., & Schaller, G. 1993, *A&AS*, 98, 523
- Schaller, G., Schaerer, D., Meynet, G., & Maeder, A. 1992, *A&AS*, 96, 269
- Schweickhardt, J., Schmutz, W., Stahl, O., Szeigfert, T., & Wolf, B. 1999, *A&A*, 347, 127
- Shu, F. H., & Lubow, S. H. 1981, *ARA&A* 19, 277
- Vacca, W. D., Garmany, C. D., & Shull, J. M. 1996, *ApJ*, 460, 914
- van den Bergh, S. 2000, *The Galaxies of the Local Group* (Cambridge: Cambridge University Press)
- van Hamme, W. 1993, *AJ*, 106, 2096
- Westerlund, B. E. 1997, *The Magellanic Clouds* (Cambridge: Cambridge University Press)
- Wolfe, R. H., Horak, H. G., & Storer, N. W. 1967, in *Modern Astrophysics*, ed. M. Hack (Paris: Gauthier Villars), 251
- Zahn, J.-P. 1975, *A&A*, 41, 329
- Zahn, J.-P. 1977, *A&A*, 57, 383

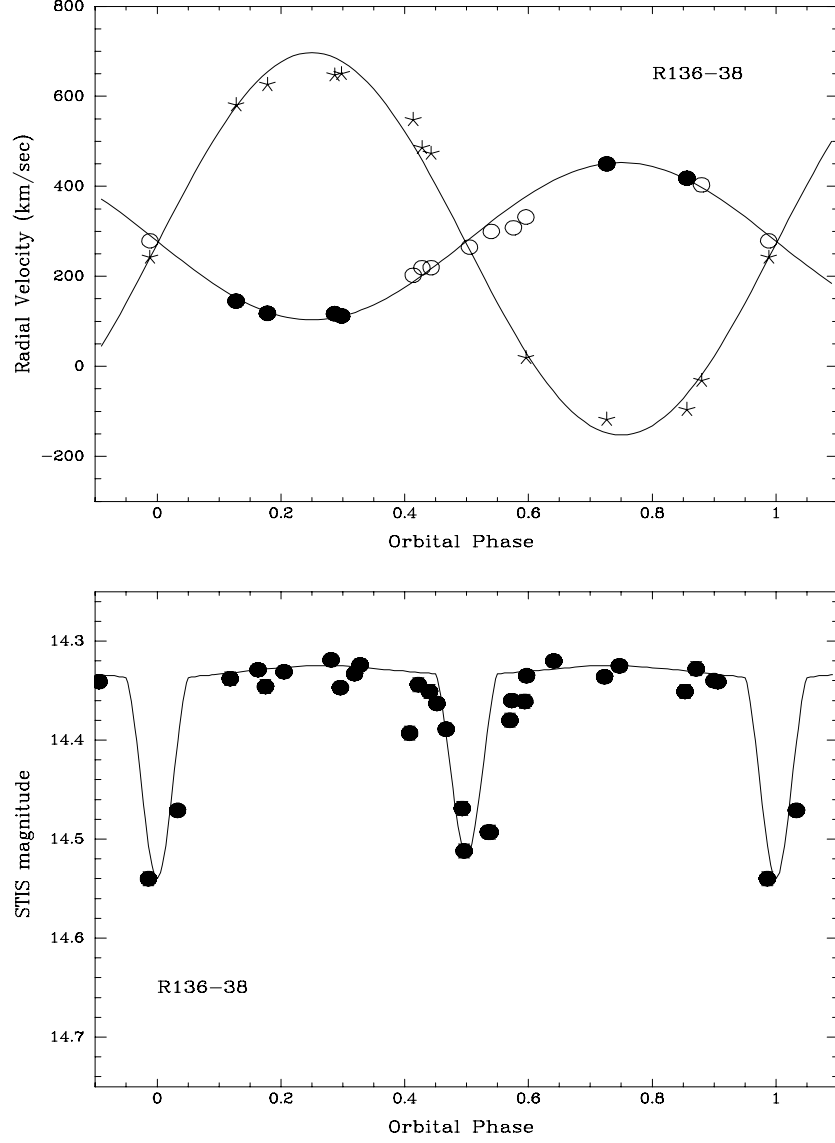


Fig. 1.— Radial velocity and light curves for R136-38. In the radial velocity curve, the solid points designate the primary; the asterisks denote the secondary, and the open circles denote the measurements at single-lined phases, which were not included in the orbit fit. In the plot of the light-curve, we include the the  $1\sigma$  error bars in the photometry, although for R136-38 these are comparable to the size of the points. The solid lines shows the results of our best model fit.

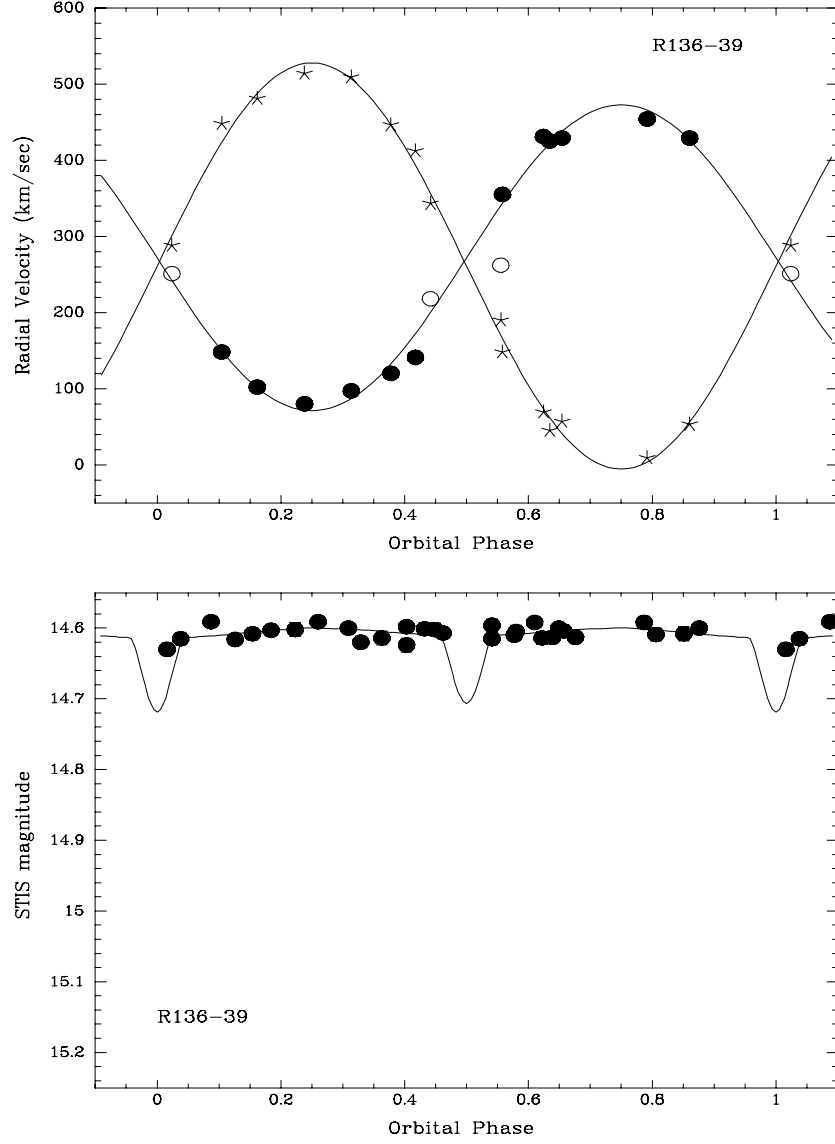


Fig. 2.— Radial velocity and light curves for R136-39; symbols are the same as in Fig. 1. The model light-curve fit is for the maximum possible eclipse depth consistent with the data; we use this for setting an upper limit on the orbital inclination.

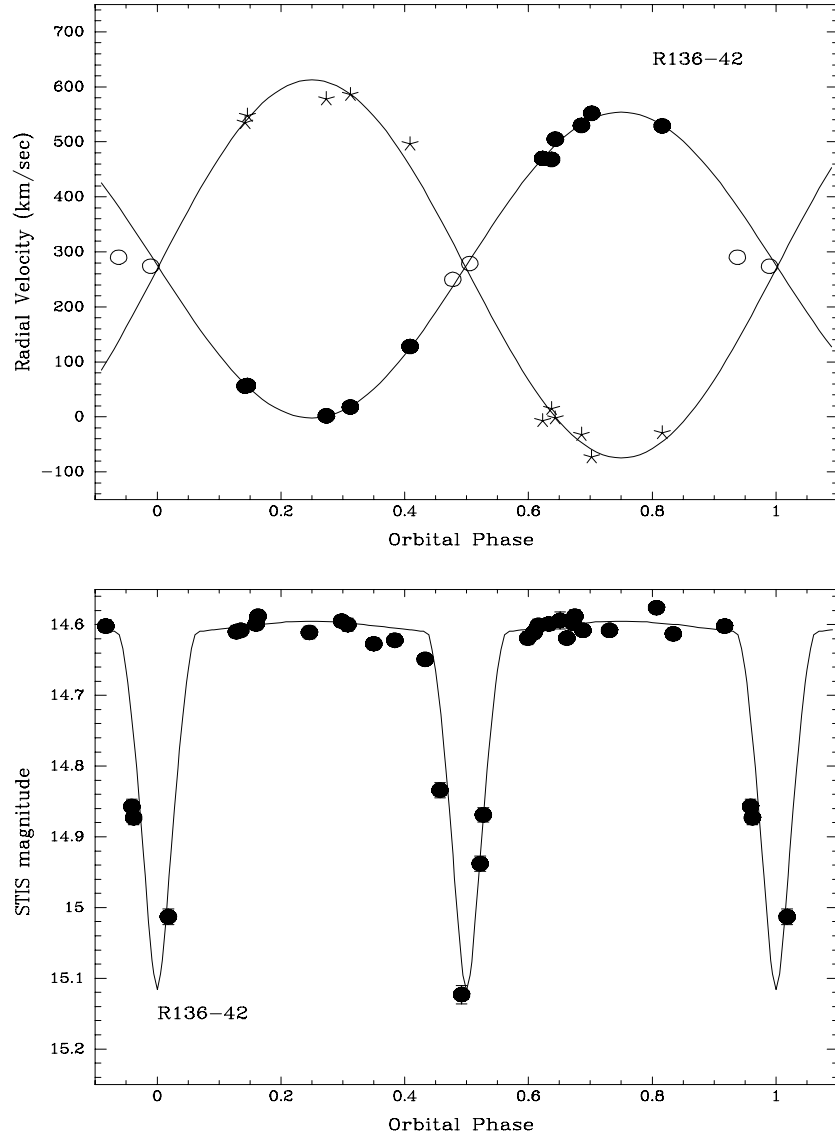


Fig. 3.— Radial velocity and light curves for R136-42; symbols are the same as in Fig. 1.

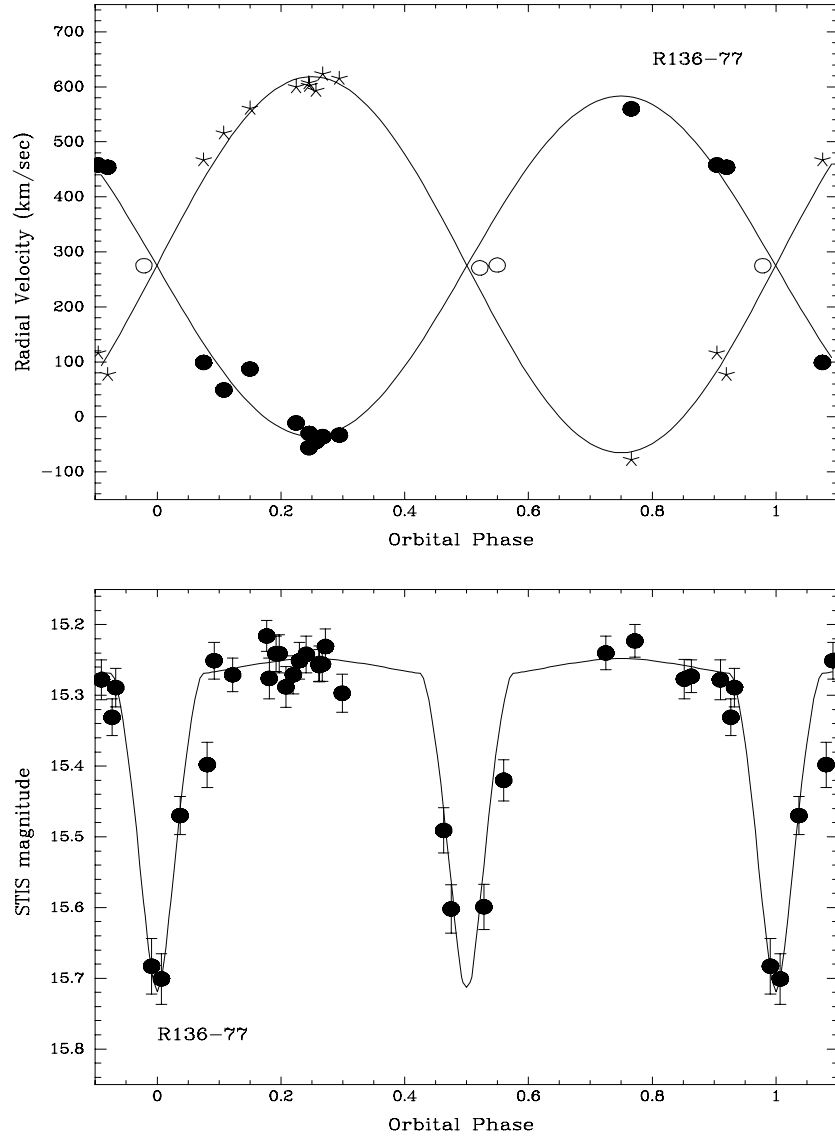


Fig. 4.— Radial velocity and light curves for R136-77; symbols are the same as in Fig. 1.

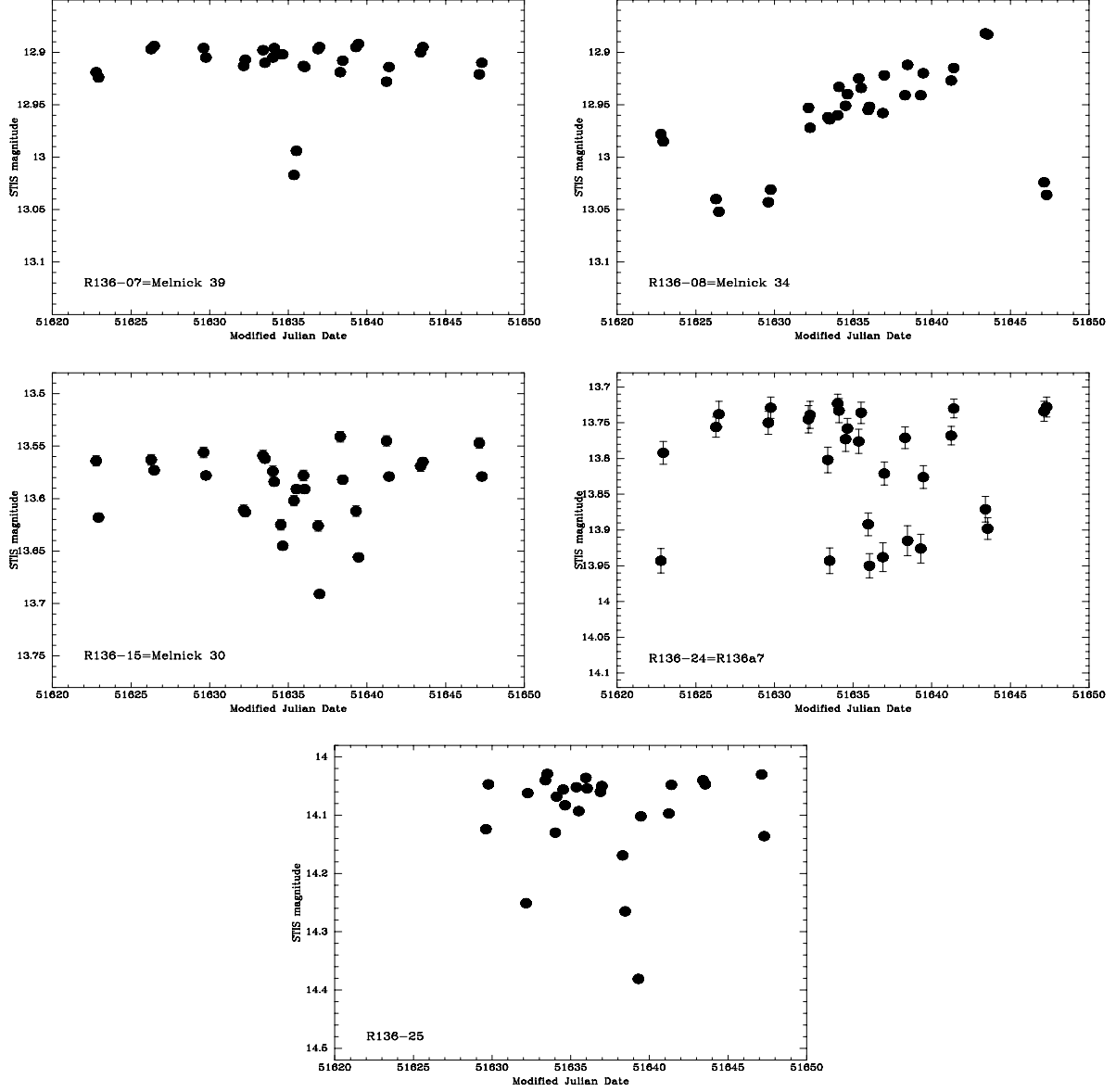


Fig. 5.— Light-curves for five other suspected binaries. R136-08 (Melnick 34) show gradual variations with a period of 20 days; the others show changes typical of eclipses.

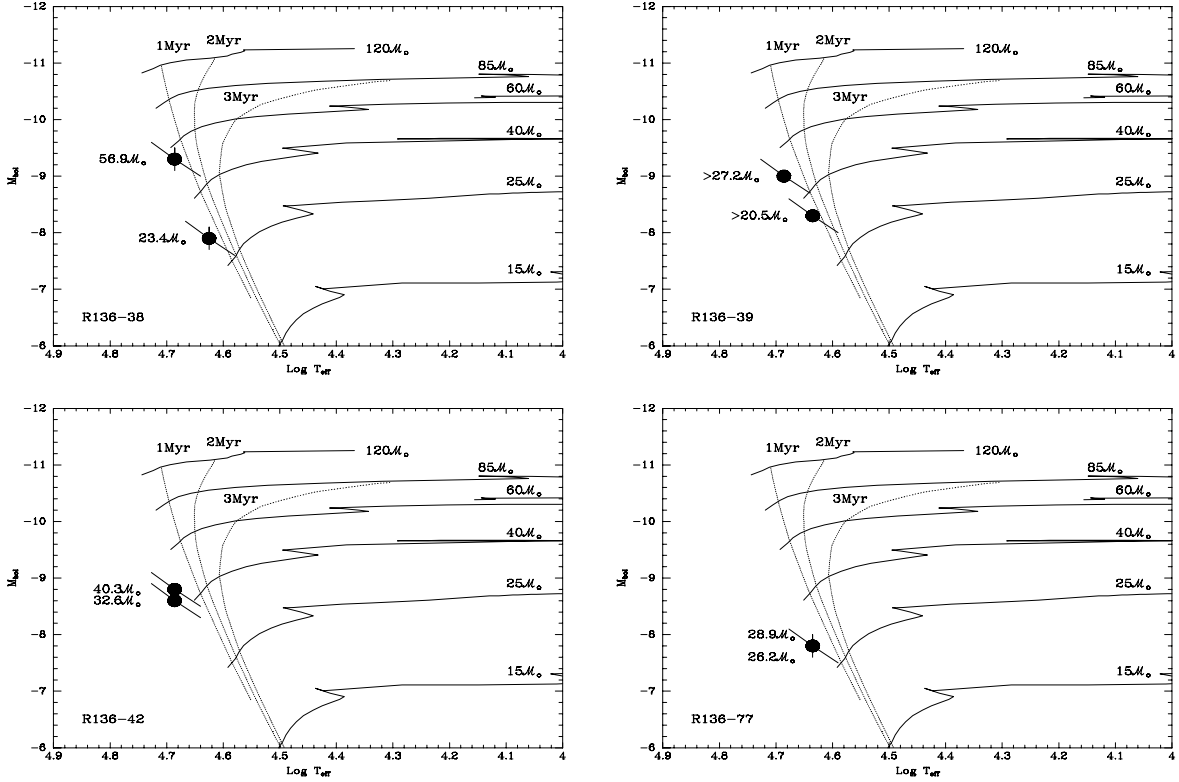


Fig. 6.— The locations of each star in the H-R diagram is shown by the large filled circles. Error bars denote the change in location due to a 5% error in the effective temperature scale, and due to uncertainties in magnitude difference in the two components. The evolutionary tracks (solid lines) are for  $z = 0.008$  and come from Schaerer et al. (1993). The dotted lines are isochrones for 1, 2, and 3 Myr, computed from the same models.

Table 1. Journal of Observations, Radial Velocities

Image Name	Modified Julian Date	Orbital Phase <sup>b</sup>	Radial Velocities (km s <sup>-1</sup> )		
			Primary	Secondary	Single
R136-38					
o59001020	51622.80	0.41	...	548	202
o59002020	51626.29	0.44	...	473	219
o59003020	51629.63	0.43	...	486	219
o59004020	51632.17	0.18	118	626	...
o59005020	51633.40	0.54	...	...	300
o59006020	51634.03	0.73	450	−118 <sup>a</sup>	...
o59007020	51634.55	0.88	...	−32	403
o59008020	51635.39	0.13	145	581	...
o59009020	51635.97	0.30	112	650	...
o59010020	51636.91	0.58	...	...	308
o59011020	51638.31	0.99	...	242	279
o59012020	51639.32	0.29	117	647	...
o59013020	51641.25	0.86	418	−96	...
o59014020	51643.45	0.51	...	...	265
o59015020	51647.15	0.60	...	19	332
R136-39					
o59001030	51622.84	0.56	...	190	262
o59002030	51626.34	0.42	141 <sup>a</sup>	412	...
o59003030	51629.67	0.24	80	514	...
o59004030	51632.20	0.86	429	53	...
o59005030	51633.42	0.16	102	481	...
o59006030	51634.04	0.31	97	509	...
o59007030	51634.56	0.44	...	343	218
o59008030	51635.42	0.65	429	57	...
o59009030	51635.98	0.79	454	9	...

Table 1—Continued

Image Name	Modified Julian Date	Orbital Phase <sup>b</sup>	Radial Velocities (km s <sup>-1</sup> )		
			Primary	Secondary	Single
o59010030	51636.92	0.02	...	288 <sup>a</sup>	251
o59011030	51638.36	0.38	120	446	...
o59012030	51639.36	0.62	431	69	...
o59013030	51641.31	0.10	148	448	...
o59014030	51643.46	0.63	425	45	...
o59015030	51647.21	0.56	355 <sup>a</sup>	148 <sup>a</sup>	
R136-42					
o59001040	51622.86	0.27	2	578	...
o59002040	51626.34	0.48	...	...	250
o59003040	51629.69	0.64	468	15	...
o59004040	51632.20	0.51	...	...	279
o59005040	51633.45	0.94	...	...	290
o59006040	51634.05	0.15	57	548	...
o59007040	51634.53	0.31	18	586	...
o59008040	51635.43	0.62	470	−7	...
o59009040	51635.99	0.82	529	−29	...
o59010040	51636.93	0.14	56	535	...
o59011040	51638.38	0.64	505	−2	...
o59012040	51639.38	0.99	...	...	274
o59013040	51641.39	0.69	530	−32	...
o59014040	51643.48	0.41	128	496	...
o59015040	51647.22	0.70	552	−73	...
R136-77					
o59001050	51622.92	0.29	−33	615	...
o59002050	51626.41	0.15	87	561	...
o59003050	51629.74	0.92	454	77	...

Table 1—Continued

Image Name	Modified Julian Date	Orbital Phase <sup>b</sup>	Radial Velocities (km s <sup>-1</sup> )		
			Primary	Secondary	Single
o59004050	51632.23	0.25	−30	602	...
o59005050	51633.47	0.90	458	116	...
o59006050	51634.07	0.22	−11	600	...
o59007050	51634.63	0.52	...	...	271
o59008050	51635.49	0.98	...	...	275
o59009050	51636.03	0.27	−36	623	...
o59010050	51636.97	0.77	560	−78	...
o59011050	51638.44	0.55	...	...	276
o59012050	51639.43	0.08	99	467	...
o59013050	51641.37	0.11	49	516	...
o59014050	51643.53	0.26	−45	593	...
o59015050	51647.27	0.25	−56	607	...

<sup>a</sup>Given half weight in orbit solution.

<sup>b</sup>Based upon the orbital parameters given subsequently.

Table 2. Journal of Observations, Photometry

Image Name	MJD	R136-38 <sup>a</sup>	R136-39 <sup>b</sup>	R136-42 <sup>c</sup>	R136-77 <sup>d</sup>
o59001010	51622.78	14.39	14.61	14.61	15.27
o59001060	51622.93	14.36	14.61	14.60	15.30
o59002010	51626.28	14.35	14.62	14.83	15.40
o59002060	51626.47	14.51	14.60	14.94	15.28
o59003010	51629.61	14.34	14.60	14.61	15.28
o59003060	51629.76	14.39	14.59	14.62	15.29
o59004010	51636.89	14.38	14.63	14.61	15.24
o59004060	51636.98	14.34	14.61	14.60	15.22
o59005010	51638.30	14.54	14.61	14.60	15.60
o59005060	51638.46	14.47	14.60	14.60	15.42
o59006010	51639.30	14.32	14.59	14.87	15.70
o59006060	51639.46	14.32	14.60	15.01	15.25
o59007010	51641.24	14.35	14.59	14.60	15.47
o59007060	51641.40	14.34	14.62	14.61	15.27
o59008010	51643.41	14.47	14.61	14.62	15.24
o59008060	51643.55	14.49	14.60	14.65	15.26
o59009010	51647.14	14.36	14.60	14.59	15.22
o59009060	51647.30	14.32	14.60	14.61	15.26
o59010010	51632.16	14.35	14.61	15.12	15.29
o59010060	51632.26	14.33	14.60	14.87	15.26
o59011010	51633.39	14.49	14.61	14.60	15.27
o59011060	51633.51	14.36	14.60	14.86	15.33
o59012010	51634.02	14.34	14.60	14.61	15.24
o59012060	51634.10	14.32	14.62	14.59	15.24
o59013010	51634.52	14.33	14.60	14.60	15.49
o59013060	51634.64	14.34	14.61	14.63	15.60
o59014010	51635.36	14.34	14.61	14.62	15.28
o59014060	51635.51	14.33	14.61	14.59	15.68
o59015010	51635.96	14.35	14.59	14.58	15.25
o59015060	51636.04	14.33	14.61	14.61	15.23

<sup>a</sup>The photometric error for R366-38 is  $1\sigma = 0.007$  mag.

<sup>b</sup>The photometric error for R366-39 is  $1\sigma = 0.009$  mag.

<sup>c</sup>The photometric error for R366-42 is  $1\sigma = 0.010$  mag.

<sup>d</sup>The photometric error for R366-77 is  $1\sigma = 0.027$  mag.

Table 3. Orbit Solutions and Physical Parameters R136-38

Parameter	System	Primary	Secondary
Orbital			
$P$ (days)	3.39 (adopted)	...	...
$e$	0.00 (adopted)	...	...
$T_{\text{p. conjunction}}$ (MJD)	$51621.40 \pm 0.03$	...	...
$\gamma$ (km s $^{-1}$ )	...	$278.2 \pm 0.4$	$272.3 \pm 0.3$
$K$ (km s $^{-1}$ )	...	$174.7 \pm 0.5$	$424.8 \pm 0.2$
$m_p/m_s$	0.41	...	...
$R_1$ (km s $^{-1}$ )	...	2.3	20.3
$a \sin i$ ( $R_o$ )	40.2	11.7	28.5
$m \sin^3 i$ ( $\mathcal{M}_\odot$ )	...	$53.8 \pm 0.2$	$22.1 \pm 0.1$
Spectral and Photometric			
Spectral Type	...	O3 V	O6 V
$T_{\text{eff}}$ (°K)	...	$48,500 \pm 4,850^{\text{a}}$	$42,200 \pm 4,220^{\text{a}}$
$\Delta m$	$1.0 \pm 0.2$	...	...
$M_V$	−5.3	$-4.9 \pm 0.2^{\text{b}}$	$-3.9 \pm 0.2^{\text{b}}$
BC	...	$-4.4 \pm 0.3^{\text{a}}$	$-4.0 \pm 0.3^{\text{a}}$
$M_{\text{bol}}$	...	$-9.3 \pm 0.4^{\text{a,b}}$	$-7.9 \pm 0.4^{\text{a,b}}$
Radius ( $R_o$ )	...	$9.3 \pm 1.0^{\text{a,b}}$	$6.4 \pm 0.7$
$v_{\text{sync}}$	...	$110 \pm 12$	$76 \pm 9$
$v \sin i$	...	$130 \pm 20$	$90 \pm 20$
Eclipse depths	...	0.23	0.20
inclination (geometry) [deg]	$79.0 \pm 1.0$	...	...
inclination (GENSYN model) [deg]	$79.0 \pm 1.0$	...	...
Masses			
$m$ ( $\mathcal{M}_\odot$ ) orbit	...	$56.9 \pm 0.6$	$23.4 \pm 0.2$
$m$ ( $\mathcal{M}_\odot$ ) evolutionary tracks	...	$53 \pm 5^{\text{c}}$	$29 \pm 2^{\text{c}}$

<sup>a</sup>Adopting a 10% uncertainty in the spectral-type to  $T_{\text{eff}}$  relationship.

<sup>b</sup>Errors (anti-)correlated.

<sup>c</sup>Errors on the masses from the evolutionary tracks are based solely on the errors in  $M_V$ .

Table 4. Orbit Solutions and Physical Parameters R136-39

Parameter	System	Primary	Secondary
Orbital			
$P$ (days)	4.06 (adopted)	...	...
$e$	0.00 (adopted)	...	...
$T_{\text{p. conjunction}}$ (MJD)	$51620.59 \pm 0.01$	...	...
$\gamma$ (km s $^{-1}$ )	...	$271.8 \pm 0.3$	$262.0 \pm 0.3$
$K$ (km s $^{-1}$ )	...	$200.8 \pm 0.5$	$266.3 \pm 0.4$
$m_p/m_s$	$0.754 \pm 0.002$	...	...
R1 (km s $^{-1}$ )	...	7.1	9.5
$a \sin i$ ( $R_o$ )	37.5	16.1	21.4
$m \sin^3 i$ ( $\mathcal{M}_\odot$ )	...	$24.5 \pm 0.1$	$18.5 \pm 0.1$
Spectral and Photometric			
Spectral Type	...	O3 V	O5.5 V
$T_{\text{eff}}$ (°K)	...	$48,500 \pm 4,850^{\text{a}}$	$43,200 \pm 4,320^{\text{a}}$
$\Delta m$	$0.45 \pm 0.1$	...	...
$M_V$	−5.2	$-4.7 \pm 0.1^{\text{b}}$	$-4.2 \pm 0.1^{\text{b}}$
BC	...	$-4.4 \pm 0.3^{\text{a}}$	$-4.1 \pm 0.3^{\text{a}}$
$M_{\text{bol}}$	...	$-9.0 \pm 0.3^{\text{a,b}}$	$-8.3 \pm 0.3^{\text{a,b}}$
Radius ( $R_o$ )	...	$8.1 \pm 0.6^{\text{a,b}}$	$7.1 \pm 0.6$
$v_{\text{sync}}$	...	$83 \pm 6$	$71 \pm 6$
$v \sin i$	...	$< 100$	$< 100$
Eclipse depths	...	$< 0.05?$	...
inclination (geometry)[deg]	$< 72.0?$	...	...
inclination (GENSYN model) [deg]	$< 75.0$	...	...
Masses			
m ( $\mathcal{M}_\odot$ ) orbit	...	$> 27.2$	$> 20.5$
m ( $\mathcal{M}_\odot$ ) evolutionary tracks	...	$46 \pm 2^{\text{c}}$	$34 \pm 2^{\text{c}}$

<sup>a</sup>Adopting a 10% uncertainty in the spectral-type to  $T_{\text{eff}}$  relationship.

<sup>b</sup>Errors (anti-)correlated.

<sup>c</sup>Errors on the masses from the evolutionary tracks are based solely on the errors in  $M_V$ .

Table 5. Orbit Solutions and Physical Parameters R136-42

Parameter	System	Primary	Secondary
Orbital			
$P$ (days)	2.89 (adopted)	...	...
$e$	0.00 (adopted)	...	...
$T_{\text{p. conjunction}}$ (MJD)	$51622.07 \pm 0.01$	...	...
$\gamma$ (km s $^{-1}$ )	...	$276.0 \pm 0.3$	$268.0 \pm 0.3$
$K$ (km s $^{-1}$ )	...	$278.2 \pm 0.4$	$343.7 \pm 0.4$
$m_p/m_s$	$0.809 \pm 0.001$	...	...
R1 (km s $^{-1}$ )	...	4.7	12.8
$a \sin i$ ( $R_o$ )	35.5	15.9	19.6
$m \sin^3 i$ ( $\mathcal{M}_\odot$ )	...	$39.9 \pm 0.1$	$32.3 \pm 0.1$
Spectral and Photometric			
Spectral Type	...	O3 V	O3 V
$T_{\text{eff}}$ (°K)	...	$48,500 \pm 4,850^{\text{a}}$	$48,500 \pm 4,850^{\text{a}}$
$\Delta m$	$0.2 \pm 0.1$	...	...
$M_V$	−5.1	$-4.4 \pm 0.1^{\text{b}}$	$-4.2 \pm 0.1^{\text{b}}$
BC	...	$-4.4 \pm 0.3^{\text{a}}$	$-4.4 \pm 0.3^{\text{a}}$
$M_{\text{bol}}$	...	$-8.8 \pm 0.3^{\text{a,b}}$	$-8.6 \pm 0.3^{\text{a,b}}$
Radius ( $R_o$ )	...	$7.4 \pm 0.8^{\text{a,b}}$	$6.7 \pm 0.7$
$v_{\text{sync}}$	...	$102 \pm 9$	$93 \pm 7$
$v \sin i$	...	$100 \pm 20$	$130 \pm 30$
Eclipse depths	...	$> 0.40$	0.52
inclination (geometry) [deg]	$85.5 \pm 1.0$	...	...
inclination (GENSYN model) [deg]	$85.4 \pm 0.5$	...	...
Masses			
m ( $\mathcal{M}_\odot$ ) orbit	...	$40.3 \pm 0.1$	$32.6 \pm 0.1$
m ( $\mathcal{M}_\odot$ ) evolutionary tracks	...	$42 \pm 2^{\text{c}}$	$39 \pm 3^{\text{c}}$

<sup>a</sup>Adopting a 10% uncertainty in the spectral-type to  $T_{\text{eff}}$  relationship.

<sup>b</sup>Errors (anti-)correlated.

<sup>c</sup>Errors on the masses from the evolutionary tracks are based solely on the errors in  $M_V$ .

Table 6. Orbit Solutions and Physical Parameters R136-77

Parameter	System	Primary	Secondary
Orbital			
$P$ (days)	1.88 (adopted)	...	...
$e$	0.00 (adopted)	...	...
$T_{\text{p. conjunction}}$ (MJD)	$51622.37 \pm 0.01$	...	...
$\gamma$ (km s $^{-1}$ )	...	$273.8 \pm 0.3$	$276.6 \pm 0.3$
$K$ (km s $^{-1}$ )	...	$309.2 \pm 0.4$	$341.9 \pm 0.3$
$m_p/m_s$	$0.904 \pm 0.001$	...	...
R1 (km s $^{-1}$ )	...	17.5	14.8
$a \sin i$ ( $R_o$ )	24.1	11.5	12.7
$m \sin^3 i$ ( $\mathcal{M}_\odot$ )	...	$28.3 \pm 0.1$	$25.6 \pm 0.1$
Spectral and Photometric			
Spectral Type	...	O5.5 V	O5.5 V
$T_{\text{eff}}$ (°K)	...	$43,200 \pm 4,320^{\text{a}}$	$43,200 \pm 4,320^{\text{a}}$
$\Delta m$	$0.0 \pm 0.2$	...	...
$M_V$	−4.5	$-3.7 \pm 0.2^{\text{b}}$	$-3.7 \pm 0.2^{\text{b}}$
BC	...	$-4.1 \pm 0.3^{\text{a}}$	$-4.1 \pm 0.3^{\text{a}}$
$M_{\text{bol}}$	...	$-7.8 \pm 0.4^{\text{a,b}}$	$-7.8 \pm 0.4^{\text{a,b}}$
Radius ( $R_o$ )	...	$5.8 \pm 0.5^{\text{a,b}}$	$5.8 \pm 0.5$
$v_{\text{sync}}$	...	$124 \pm 13$	$124 \pm 13$
$v \sin i$	...	$140 \pm 20$	$130 \pm 20$
Eclipse depths	...	0.45	$> 0.35$
inclination (geometry) [deg]	$83.0 \pm 1.0$	...	...
inclination (GENSYN model) [deg]	$83.0 \pm 1.0$	...	...
Masses			
m ( $\mathcal{M}_\odot$ ) orbit	...	$28.9 \pm 0.3$	$26.2 \pm 0.3$
m ( $\mathcal{M}_\odot$ ) evolutionary tracks	...	$28 \pm 1^{\text{c}}$	$28 \pm 0.1^{\text{c}}$

<sup>a</sup>Adopting a 10% uncertainty in the spectral-type to  $T_{\text{eff}}$  relationship.

<sup>b</sup>Errors (anti-)correlated.

<sup>c</sup>Errors on the masses from the evolutionary tracks are based solely on the errors in  $M_V$ .